Article

Screening and Druggability Analysis of Marine Active Metabolites against SARS-CoV-2: An Integrative Computational Approach

Selvakumar Murugesan [1], Chinnasamy Ragavendran [2], Amir Ali [2,3,4,5,*], Velusamy Arumugam [6], Dinesh Kumar Lakshmanan [6], Palanikumar Palanichamy [7], Manigandan Venkatesan [8,*], Chinnaperumal Kamaraj [9], Juan Pedro Luna-Arias [3,4], Fernández-Luqueño Fabián [3], Safir Ullah Khan [4], Zia ur-Rehman Mashwani [5] and Muhammad Younas [5]

[1] Department of Biotechnology, BIT Campus, Anna University, Tiruchirappalli 620024, India
[2] Department of Conservative Dentistry and Endodontics, Saveetha Dental College and Hospitals, Saveetha Institute of Medical and Technical Sciences (SIMATS), Chennai 600077, India
[3] Nanoscience and Nanotechnology Program Center for Research and Advanced Studies, National Polytechnic Institute, Mexico City 07360, Mexico
[4] Department of Cell Biology, Center for Research and Advanced Studies of the National Polytechnic Institute, Av. Instituto Politécnico Nacional 2508, Col. San Pedro Zacatenco, Mexico City 07360, Mexico
[5] Department of Botany, PMAS, Arid Agriculture University, Rawalpindi 46000, Pakistan
[6] Department of Environmental Biotechnology, Bharathidasan University, Tiruchirappalli 620024, India
[7] Department of Genomics, School of Biological Sciences, Madurai Kamaraj University, Madurai 625021, India
[8] Department of Medicine, University of Texas Health Science Center, Sanantonio, TX 78284, USA
[9] Interdisciplinary Institute of Indian System of Medicine (IIISM), Directorate of Research, SRM Institute Science and Technology, Kattankulathur, Chennai 603203, India
* Correspondence: ali.amir@cinvestav.mx (A.A.); venkatesanm@uthscsa.edu (M.V.)

Abstract: Severe acute respiratory syndrome coronavirus 2 (SARS-CoV-2) infections have triggered a recent pandemic of respiratory disease and affected almost every country all over the world. A large amount of natural bioactive compounds are under clinical investigation for various diseases. In particular, marine natural compounds are gaining more attention in the new drug development process. The present study aimed to identify potential marine-derived inhibitors against the target proteins of COVID-19 using a computational approach. Currently, 16 marine clinical-level compounds were selected for computational screening against the 4 SARS-CoV-2 main proteases. Computational screening resulted from the best drug candidates for each target based on the binding affinity scores and amino acid interactions. Among these, five marine-derived compounds, namely, chrysophaentin A (-6.6 kcal/mol), geodisterol sulfates (-6.6 kcal/mol), hymenidin (-6.4 kcal/mol), plinabulin (-6.4 kcal/mol), and tetrodotoxin (-6.3 kcal/mol) expressed minimized binding energy and molecular interactions, such as covalent and hydrophobic interactions, with the SARS CoV-2 main protease. Using molecular dynamic studies, the root-mean-square deviation (RMSD), root-mean-square fluctuation (RMSF), radius of gyration (ROG), and hydrogen bond (H-Bond) values were calculated for the SARS-CoV-2 main protease with a hymenidin docked complex. Additionally, in silico drug-likeness and pharmacokinetic property assessments of the compounds demonstrated favorable druggability. These results suggest that marine natural compounds are capable of fighting SARS-CoV-2. Further in vitro and in vivo studies need to be carried out to confirm their inhibitory potential.

Keywords: COVID-19; molecular docking; ADMET; marine natural products; chrysophaentin A; hymenidin

1. Introduction

COVID-19 is one of the important epidemic diseases caused by the coronavirus (SARS-CoV-2) in the current century. It has spread to more than 210 countries, and more

than 63 crore people are affected by this disease as of October 2022 (http://www.who.int accessed on 30 Junuary 2020). In addition, SARS-CoV-2 is a current major challenge for researchers, and they are still working on the development of antiviral drugs against SARS-CoV-2 [1,2]. Recently, Veklury (remdesivir) and Olumiant (baricitinib) were officially approved by the FDA for the treatment of COVID-19 [3–5]. The main symptoms of SARS-CoV-2 include body aches, chest pain, chills with shaking, dry cough, fever, nausea, shortness of breath, and trouble breathing [6,7]. It primarily affects the respiratory pathway system, infects the lung endothelial cells, and induces inflammatory cell invasion and lymphocytic endothelialitis at the pathological state [8]. SARS-CoV-2 viruses are RNA-based viruses (single-stranded) found in several animal species. The size of the viral genome is nearly 30 kb with a $5'$-cap and $3'$-poly(A) tail. It contains four structural coding genes: spike, envelope, membrane, and nucleocapsid genes [9,10]. It encodes various structural/non-structural proteins (Nsps), which are produced as cleavage end products of the viral polyproteins (ORF1a and ORF1ab) [11]. In total, 16 Nsps are present in the SARS-CoV-2 viral genome, and each has some specific function such as Nsp1 and Nsp2 suppress the expression of the host gene; Nsp3, the formation of multidomain complexes; Nsp4 and Nsp6, in the transmembrane, protein activity; Nsp5, protease activity; Nsp7 and Nsp8, the primase enzyme; Nsp9, the dimerization of RNA; Nsp10, the activation of a replicative enzyme; Nsp12, RNA polymerase activity [12]; Nsp13, helicase activity; Nsp14: exoribonuclease activity; Nsp15, endonuclease activity; and Nsp16, methyltransferase activity [13,14].

Initially, the viral particles enter the host cell and bind to the enterocytes and pneumocytes. After the replication process, the viral particles are formed and spread into other cells such as the cerebral neuronal, immune, and tubular epithelial cells. The spike protein is used to attach to the host cell protein, and it interacts with the angiotensin-converting enzyme-2 (ACE-2) [15,16]. Once the viral particles enter the host cells, they are released into the genome along with the nucleocapsid. ORF1a and ORF1ab produce two polyproteins, pp1a and pp1b, which enable the translation process using the ribosome of the host cell. Both the pp1a and pp1b polyproteins help to form a replication/transcription complex [17]. Currently, researchers and scientists are working on the development of a drug against COVID-19 in the following ways such as the prevention of self-assembly (structural proteins), viral replications (Nsps), viral entry, and the blocking of the signaling pathways required for viral infections [18].

The marine environment possesses various spectra of species (i.e., animals and plants, such as seaweeds), which contribute to yielding major economic growth across the globe [19]. Marine algae, corals, jellyfish, sharks, seaweeds, and sponges are potentially active renewable resources, and they have been used for food, medicine, and nutraceutical prospects around the world [20]. Recently, biomedical researchers have been focusing on drug discovery using natural sources, such as marine natural products (MDPs), in particular. Numerous MDPs have been reported as having various pharmacological and biological activities such as antibiotic, anticancer, anti-inflammatory, antiviral, and neuroprotective properties. Cytarabine (Ara-C) is the first marine-derived anticancer agent, isolated from marine sponges, and it blocks the DNA polymerase function in cancer cells. It was approved for the treatment of leukemia by the FDA in 1969 [21]. In total, 18 MDPs are involved in clinical trials (Phase I: four, Phase II: eight, and Phases III and IV: six), and four marine-derived compounds (brentuximab vedotin, cytarabine, eribulin mesylate, trabectedin) have been approved and are available in the market. The pharmaceutical pipeline comprising approved and developmental MDPs offers new hopes and new tools in the treatment of COVID-19 patients. The findings of the present study will deliver valuable data for the development of MDP derivatives as lead structures and novel therapeutic and prophylaxis drug candidates against COVID-19 in the near future.

2. Materials and Methods

2.1. Software/Servers Used

The marine preclinical- and clinical-level bioactive compounds are listed using PubMed database. All marine bioactive compound structures were collected from PubChem database. Protein structures were obtained from RCSB protein data bank. DruLiTo 1.0.0 software was used to analyze the physiochemical properties of marine bioactive compounds. pkCSM, a pharmacokinetics online server, was used to predict the ADMET properties, Open Babel v.2.3 and PyRx 0.8 were used for molecular docking studies, and the post-docking studies were carried out using Discovery studio 2017R2.

2.2. Target Protein Preparation

The 3D crystal structures of SARS-CoV-2 main protease (6LU7; 2.16 Å) were collected from the protein data bank (https://www.rcsb.org/ accessed on 5 February 2020). The unnecessary molecules, such as ions, inhibitors, ligands, heteroatoms, and water molecules, were removed from the COVID-19 target protein structure using BIOVIA Discovery Studio. The target protein structures were loaded in PyRx version 0.8 and converted into PDBQT format [22].

2.3. Ligand Preparation

The marine active compounds (preclinical and clinical levels) were used for ligand preparation (Table 1). The 3D structures of the selected marine bioactive compounds were collected from the PubChem database (https://pubchem.ncbi.nlm.nih.gov/ accessed on 5 February 2020) in SDF file format. Initially, the ligand files were loaded, and energy was minimized using Open Babel (MMFF94 method). After the energy minimization process, the ligand files were converted into PDBQT format. These energy-minimized ligands were subjected to further docking analysis [23].

2.4. Drug-Likeness Calculations

The drug-likeness analysis was performed to analyze the structural and physicochemical properties of potent hits such as atom molar refractivity (AMR), octanol–water partition coefficient (AlogP), H-bond acceptor (HBA), H-bond donor (HBD), partition coefficient (logP), molecular weight (MW), number of rotatable bonds (nRB), number of atoms, total polar surface area (TPSA), etc., using DruLiTo software. The different molecular property filters such as CMC-50-like rule [AlogP (1.3–4.1); molecular refractivity (70–110); molecular weight (230–390); number of atoms (30–55)], BBB likeness [No. of hydrogen bonds (8–10); molecular weight (400-500); no acids], Ghose filter [logP (−0.4–5.6); molar refractivity (40–130); molecular weight (160–480); number of atoms (20–70); polar surface area < 140], MDDR-like rule [No. of rings $\geq$ 3; No. of rigid bonds $\geq$ 18; No. of rotatable bonds $\geq$ 6], QED rule [molecular weight; AlogP; No. of hydrogen-bond acceptors; No. of hydrogen-bond donors; No. of rotatable bonds; polar surface area; No. of aromatic bond count; No. of structural alerts], and Veber rule [No. of rotatable bonds $\leq$ 10; polar surface area $\leq$ 140] were applied [24].

2.5. Prediction of Pharmacokinetic Parameters

In silico ADMET (absorption, distribution, metabolism, excretion, and toxicity) analysis was performed to analyze the pharmacokinetic properties of the potent hits, such as absorption (water solubility, intestinal absorption, Caco-2, and skin permeability), distribution (blood–brain barrier (BBB), central nervous system (CNS) permeability, and volume of distribution at steady-state (VDss)), metabolism, excretion (drug clearance), and toxicity (LD50, AMES, chronic acute, and hepatotoxicity) using the pkCSM online server (https://biosig.lab.uq.edu.au/pkcsm/ accessed on 5 February 2020) [25].

Table 1. Physiochemical properties of marine-derived clinical-level compounds using DruLiTo software.

Compound	MW	logP	AlogP	HBA	HBD	TSPA	AMR	nRB	nAtom	RC	n RigidB	nArom Ring	nHB
Cytarabine, ara-C	243.09	−2.193	−2.942	8	4	128.61	52.82	2	30	2	16	0	12
Vidarabine, ara-A	267.1	−2.367	−3.453	9	4	136.26	62.91	2	32	3	19	2	13
Tetrodotoxin	319.1	−3.581	−4.239	11	8	190.25	61.71	1	39	4	24	0	19
DMXBA	308.15	1.262	−0.538	4	0	43.18	97.19	4	43	3	21	2	4
Plinabulin	336.16	3.008	0.565	6	3	82.59	102.06	3	45	3	24	2	9
Pseudopterosin A	432.25	4.368	0.885	6	4	99.38	119.61	3	67	4	31	1	10
Chrysophaentin A	676.02	5.424	3.052	8	6	139.84	187.65	0	68	5	48	4	14
Phenethylamine	121.09	1.106	0.725	1	1	26.02	43.12	2	20	1	7	1	2
Geodisterol sulfates	506.27	5.203	1.597	6	3	112.44	139.82	7	77	4	31	1	9
Bromophycolides	662.02	6.273	4.125	4	2	66.76	145.79	1	71	3	35	1	6
Plakortin	312.23	5.484	0.253	4	0	44.76	80.06	9	54	1	13	0	4
Homogentisic acid	168.04	0.036	−0.123	4	3	77.76	44.72	2	20	1	10	1	7
Hymenidin	309.02	0.93	−1.68	6	4	91.54	72.63	5	30	2	14	2	10
Dysidine	451.2	6.237	0.807	7	3	129.15	120.8	6	64	3	27	0	10
Capnellene	220.18	3.585	1.41	1	1	20.23	65.87	0	40	3	18	0	2
Pulicatin A	223.07	0.881	0.66	3	2	78.12	65.21	2	28	2	14	1	5

MM: molecular mass, HBD: hydrogen bond donors, HBA: hydrogen bond acceptors, PSA: polar surface area, AMR: atom molar refractivity, nRB: number of rotatable bonds (MM less than 500 Da, no more than 5 HBD, no more than 10 HBA, and partition coefficient (logP) no greater than 5, TPSA no greater than 140 Å2, AMR: 40 to 130, nRB: not more than 3 RB).

2.6. Molecular Docking Studies

Following ligand and protein preparation, molecular docking was performed based on the grid box approach (X = −26.28, Y = 12.60, Z = 58.97) using AutoDock Vina inbuild PyRx version 0.8 (Dallakyan and Olson, 2015). The docking analysis of COVID-19 proteins with bioactive drug candidates was evaluated using the binding affinities (kcal/mol). After docking analysis, the docked complex files were subjected to interaction studies. The protein and the ligand complex were loaded in the BIOVIA Discovery Studio, and different types of interactions such as covalent, carbon–hydrogen (C-H), hydrophobic interactions, and van der Waal attractions were analyzed [26,27].

2.7. Molecular Dynamic Simulation

MD simulation for the target SARS-CoV-2 main protease and hymenidin was carried out for 50 ns using WebGRO online server (https://simlab.uams.edu/index.php accessed on 5 February 2020). The lowest binding energy (most negative) docking conformation generated by AutoDock Vina inbuild PyRx was taken as the initial conformation for MD simulation. Initially, the hymenidin topology file was prepared using PRODRG server (http://davapc1.bioch.dundee.ac.uk/cgi-bin/prodrg accessed on 5 February 2020). The GROMOS96 43a1 force field was used for this study, and the SARS-CoV-2 main protease and hymenidin files' energy was minimized using steepest descents for 50,000 steps [28]. The calibration of NVT/NPT was completed at 300 K and 1 bar pressure. From the MD simulation, the root-mean-square deviation (RMSD), root-mean-square fluctuation (RMSF), radius of gyration (ROG), and hydrogen bond (H-Bond) values were examined for SARS-CoV-2 main protease and hymenidin docked complex [29].

3. Results and Discussion

MDPs have been used as both nutraceutical and medicinal agents for the treatment of various health illnesses. In particular, marine secondary metabolites play an important role in pharmacological research. Drug-likeness properties are important features for drug design [30]. Moreover, the rapid development of high throughput screening (computational approaches) to rational drug design and new bioactive molecules from natural sources was an activity of the past. In total, 16 clinical and preclinical bioactive compounds from the marine ecosystem were selected for the present study (Figure 1).

3.1. Drug-Likeness Properties

The physicochemical properties, including lipophilicity, hydrogen bonding, and compound molecular weight (MW), are important in the drug development process; indeed, they influence the pharmacokinetic properties of the drug compound, including absorption, membrane permeability, distribution, drug clearance, etc [31]. Initially, all of the compounds were subjected to drug-likeness analysis. Among these compounds, 11 bioactive compounds (bromophycolides, capnellene, Cytarabine, ara-C, DMXBA, homogentisic acid, hymenidin, phenethylamine, plinabulin, pseudopterosin A, pulicatin A, vidarabine, ara-A) obeyed Lipinski's rule (Table 1). Similarly, 9 compounds (pulicatin A, capnellene, DMXBA, homogentisic acid, hymenidin, plakortin, plinabulin (NPI-2358), pseudopterosin A, β-carboline) obeyed Ghose's rule, and 6 compounds (pulicatin A, capnellene, DMXBA, phenethylamine, plakortin, β-carboline) followed the BBB likeness rule. Except for the alkaloid class of plinabulin, the other compounds did not follow the CMC-50-like rule. All of the marine drug compounds obeyed the CMC-50-like rule except tetrodotoxin. Similarly, chrysophaentin A and tetrodotoxin also did not follow the QED rule. In addition, except dysidine and the geodisterol sulfates, all of the remaining compounds did not obey the MDDR-like rule [24]. The physiochemical properties of bioactive agents are an important determinant of their permeability and lipophilicity [32].
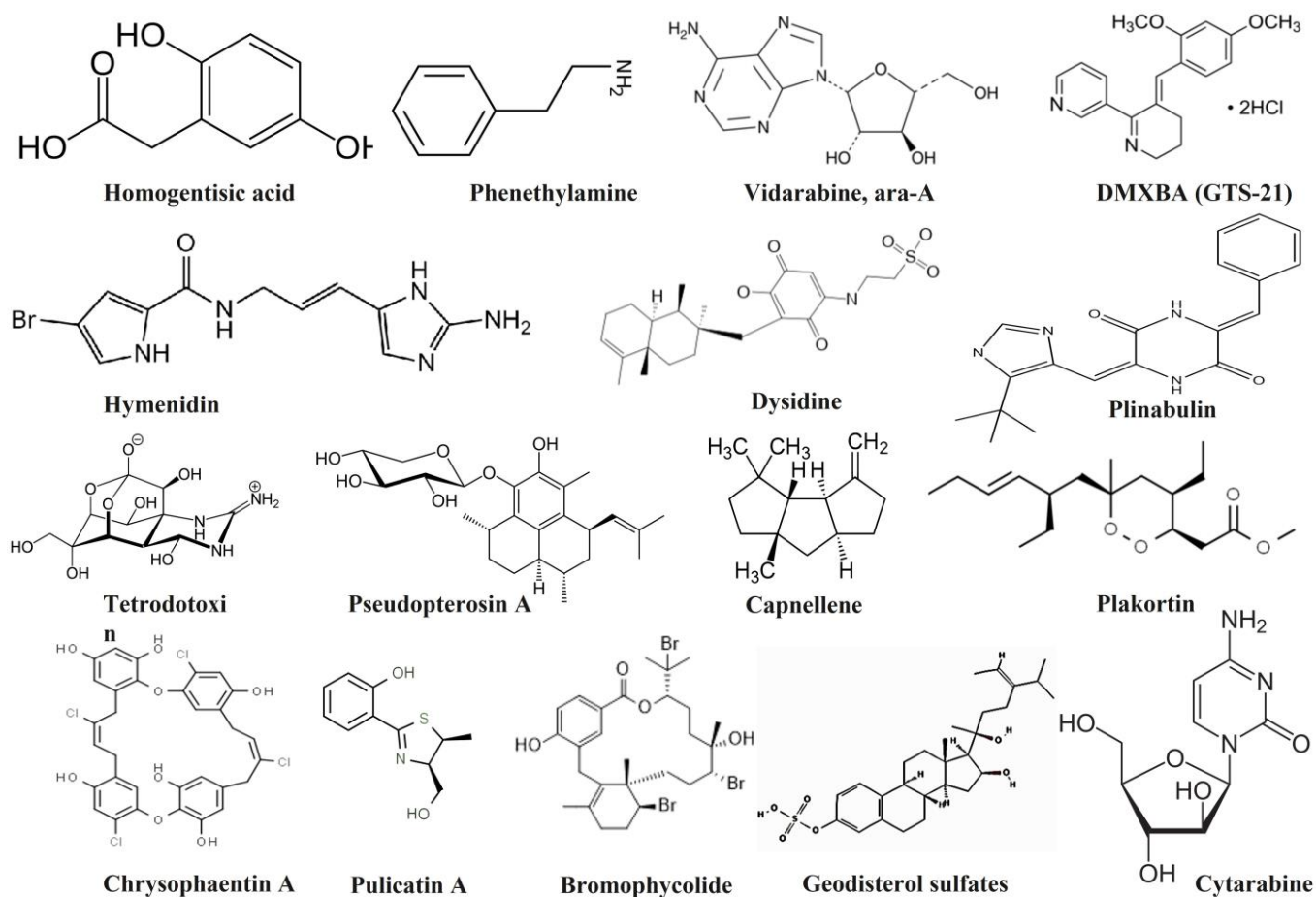
Figure 1. List of marine-derived preclinical- and clinical-level compounds.

3.2. Molecular Docking Studies

The SARS-CoV-2 main protease is an important enzyme mainly involved in replication within the host system. To inhibit this enzyme activity, viral replication should be prevented [33,34]. As no homolog of the SARS-CoV-2 main protease has been identified in humans, it is achievable to develop effective and specific SARS-CoV-2 main protease inhibitors with extremely weak inhibitory activities on human proteases, thereby reducing the side effects caused by the SARS-CoV-2 main protease inhibitors [33,35]. It contains three domains: Domain I (8–101), Domain II (102–184), and Domain III (201–303). Domain I and Domain II have an antiparallel β-barrel structure, and Domain III has five α-helices. The substrate-binding site of the SARS-CoV-2 main protease is located between Domain I and Domain II.

The marine-derived preclinical, clinical, and approved drug candidates were docked with the SARS-CoV-2 main protease using PyRx version 0.8, and the results were tabulated (Table 2). The geodisterol sulfates and chrysophaentin A were tightly bound to the COVID-19 targets of the main protease complex with minimized binding energy (−6.6 kcal/mol). Plinabulin and the hymenidin bioactive docked complex expressed the second highest binding affinity (−6.4 kcal/mol) compared with the other drug molecules. The molecular docking results were compared to standard hydroxychloroquine (HCQ) and paracetamol (Table 2).

Table 2. The binding energy values of the marine-derived clinical-level compounds to the SARS-CoV-2 main protease using PyRx version 0.8 (unit: kcal/mol).

S. No	Compound Name	PubChem ID	Chemical Class	Main Protease (6LU7)
1	Homogentisic acid	780	Phenolics	−5.6
2	Phenethylamine	1001	Alkaloid	−4.8
3	Cytarabine, ara-C	6253	Nucleoside	−6.2
4	Vidarabine, ara-A	21704	Nucleoside	−6.1
5	DMXBA (GTS-21)	5310985	Alkaloid	−5.5
6	Hymenidin	6439099	Alkaloid	−6.4
7	Plinabulin	9949641	Alkaloid	−6.4
8	Dysidine	10321583	Terpene	−5.9
9	Tetrodotoxin	11174599	Alkaloid	−6.3
10	Pseudopterosin A	11732783	Glycoside	−6.3
11	Capnellene	14060593	Terpene	−6.0
12	Bromophycolides	21778345	Terpene	−6.0
13	Geodisterol sulfates	44254699	Steroid	−6.6
14	Plakortin	44417613	Polyketide	−5.4
15	Chrysophaentin A	46872004	Shikimate	−6.6
16	Pulicatin A	136020617	Alkaloid	−5.5
17	Paracetamol	1983	Standard drug	−6.2
18	HCQ	3652	Standard drug	−6.6

The virtual screening used the receptor grid docking at the cleft of the Domain I and Domain II active sites. The geodisterol sulfates (marine steroidal compounds) and SARS-CoV-2 main protease complex showed four hydrophobic interactions (Pi-Sigma: VAL104; 3.857 Å, Alkyl: VAL104; 4.436 Å, VAL104; 4.242 Å, Pi-Alkyl: PHE294; 4.412 Å) with Domain I and Domain III. The docked complex of chrysophaentin A and the SARS-CoV-2 main protease formed three hydrogen bond interactions (GLU290; 2.576 Å, LYS137 2.938 Å, LYS5; 3.099 Å), two alkyl hydrophobic interactions (LYS137 4.531 Å, TYR126 4.243 Å), and one electrostatic interaction with the amino acid LYS137 (4.561 Å) with all domains. Hymenidin is an alkaloid class of marine bioactive compound bound to the SARS-CoV-2 main protease which showed the highest covalent interactions with a suitable binding affinity (−6.4 kcal/mol). Hymenidin interacted with the SARS-CoV-2 protease by forming four hydrogen bond interactions with the amino acids of SER158 (2.466 Å), ASP153 (2.359 Å), ASN151 (2.461 Å), and ASP295 (2.324 Å), and two hydrophobic interactions with the amino acid of VAL104 (3.809; Alkyl and 4.539; Pi-Alkyl) with Domain II and Domain III (Figure 2). Plinabulin also an alkaloid class of marine bioactive compound, bound complex exhibited one H-bond interaction (GLN110; 2.502 Å), one C-H interaction (GLN110; 3.497 Å), and two hydrophobic interactions (Pi-Sigma: THR111; 3.638 Å, Pi-Alkyl: PHE294; 4.464 Å). The alkaloid class of tetrodotoxin with the SARS-CoV-2 main protease complex showed one H-bond interaction (ASN151; 2.67 Å) and two electrostatic interactions (ASP153; 5.335 Å, PHE 294; 4.993 Å). HCQ is an anti-malarial drug which has been suggested for the treatment of COVID-19. HCQ with the SARS-CoV-2 main protease docked complex showed two H-bond interactions (GLN110; 2.608 Å, THR111; 2.187 Å) and 231 four hydrophobic bonding (ILE106; 3.686 Å, VAL101; 5.298 Å, VAL104; 4.594 Å) with 232 significant binding energy (−6.6 kcal/mol). In addition, the alkaloid class of plinabulin was also bound to the same binding region of the SARS-CoV-2 main protease (GLN110, THR111). Paracetamol can help to relieve the symptoms associated with COVID-19. The protein–ligand interaction of paracetamol and the SARS-CoV-2 main protease formed three

hydrogen bond interactions (THR111; 234 2.925 Å, ASN151; 3.083 Å, ASP295; 2.73 Å) to the amino acid residues. Similarly, the alkaloid class of hymenidin was also bound to the same binding region of the SARS-CoV-2 main protease (ASN151, ASP295) (Table 3).
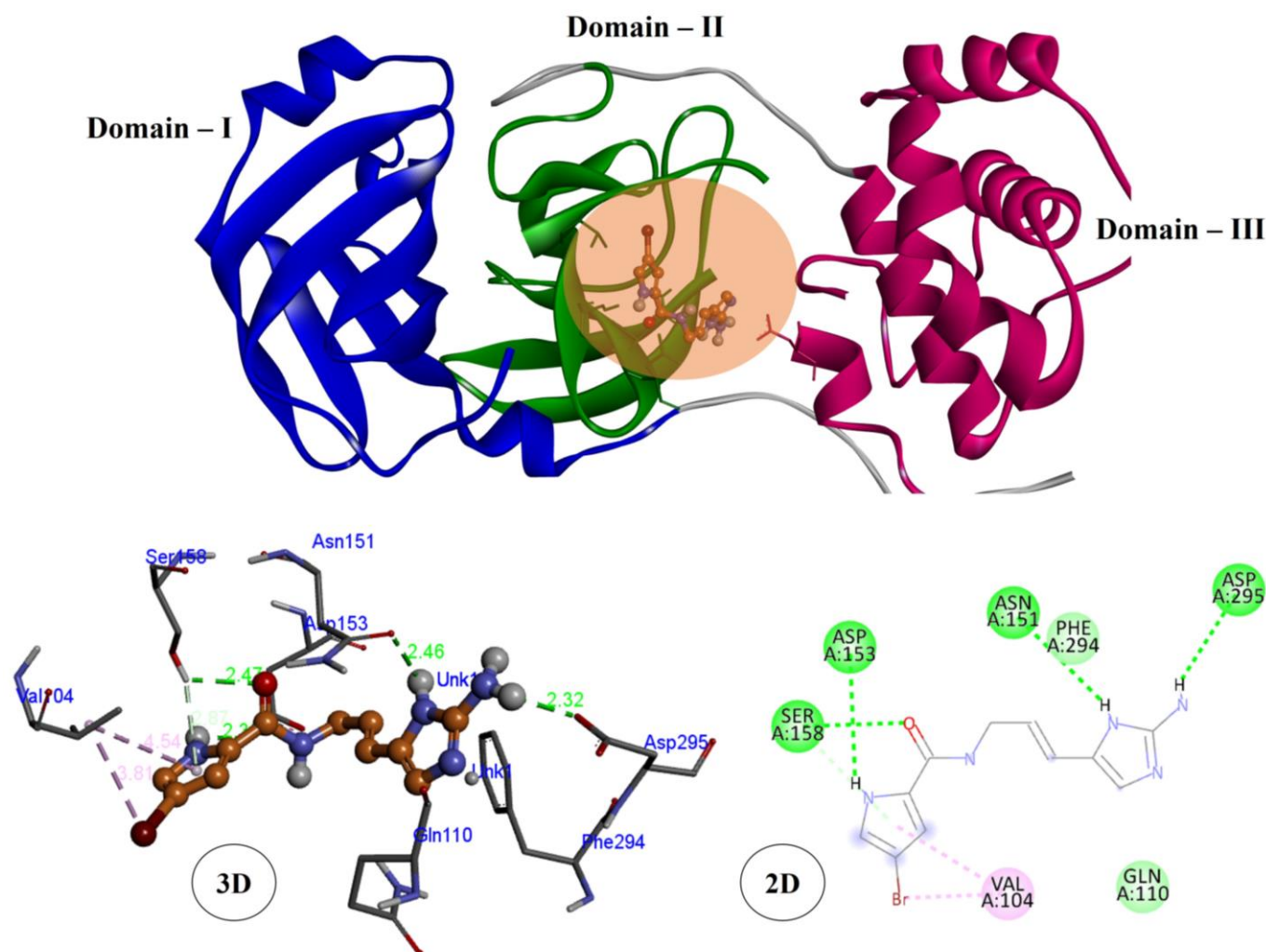

Figure 2. Non-covalent interactions and hydrogen bonding surface map between SARS-CoV-2 main protease enzyme and marine clinical-level compound (hymenidin).

Table 3. Molecular interactions of the selected marine-derived clinical-level compounds with the SARS-CoV-2 main protease using Discovery Studio 2017R2.

Compound Name	Main Protease (6LU7)
Geodisterol sulfates	VAL104, PHE294
Chrysophaentin A	GLU290, LYS137, LYS5, TYR126
Hymenidin	SER158, ASP153, ASN151, ASP295, VAL104
Plinabulin (NPI-2358)	GLN110, THR111, PHE294
Tetrodotoxin	ASN151, ASP153, PHE 294
Paracetamol	THR111, ASN151, ASP295
HCQ	GLN110, THR111, ILE106, VAL101, VAL104

Mainly found in *Ecklonia cava* (brown algae), 7,2''-Bieckol (MW 742.5) is a phlorotannin. The docking results of 7,2''-Bieckol and the SARS-CoV-2 main protease showed the lowest binding energy (−10.78 kcal/mol) compared with the standard drugs lopinavir

(−9.23 kcal/mol) and remdesivir (−9.00 kcal/mol) using MOE 2016.0802. This protein–ligand complex showed four H-bond formations (THR24, THR26, GLY143, AND GLU189), and the drug compound is mainly involved in Domain I and Domain II [36]. Similarly, the hymenidin docked complex also displayed four H-bond interactions in Domain II and Domain III. Avarol, a sesquiterpenoid hydroquinone found in Dysidea avara (sponge), is mainly used as an antiviral agent. Avarol and the SARS-CoV-2 main protease displayed one H-bond interaction (GLN 189) and seven hydrophobic interactions (HIS41, HIS164, MET49, MET165, CYS44, ASP187, ARG188) in Domain I and Domain II. The chrysophaentin A docked complex exhibited three hydrogen bond interactions (GLU290, LYS137, LYS5), two alkyl hydrophobic interactions (LYS137, TYR126), and one electrostatic interaction with the amino acid (LYS137) with all domains (I, II, and III) [37]. There were molecular docking studies for the SARS-CoV-2 main protease and *Clathria* sp. (marine sponge) natural compounds (clathrin-A, −6.67 kcal/mol; clathrin-B, −7.09 kcal/mol; clathsterol, −2.20 kcal/mol; and mirabilin-G, −7.38 kcal/mol). Among these four compounds, clathsterol showed four H-bond formations (CYS145, HIS163, THR26, GLY143), and mirabilin-G showed one H-bond formation (GLU166) in Domain I and Domain II [38]. According to [39,40], the docking studies for 57 antiviral marine alkaloids with the SARS-CoV-2 main protease, 2 marine alkaloids (manzamine A, −10.2 kcal/mol and 8-hydroxymanzamine, −10.5 kcal/mol) displayed minimized binding energy in Domain II compared to the standard drugs (darunavir, −7.9 kcal/mol and lopinavir, −7.4 kcal/mol) against the SARS-CoV-2 main protease.

3.3. Molecular Dynamics Simulation

MD simulation is a computer-based approach used to predict the stability of the protein–ligand complexes, conformational flexibilities, and the dependability of protein–ligand affinities [41]. Therefore, a marine active compound of hymenidin with a low SARS-CoV-2 main protease docking score was submitted for MD simulations followed by binding energy calculations.

Root-mean-square deviation (RMSD) is used to examine the conformational stability of the protein–ligand complex (SARS-CoV-2 main protease–hymenidin), and it is defined as the "square root of an average value of the square of coordinate values of the protein". High values of RMSD represent the conformational instability of the docked complex. In general, the RMSD value should be 2 to 3 Å. In the present study, the SARS-CoV-2 main protease–hymenidin docked complex showed less than 3 Å RMSD value (0.1 to 0.3 nm) until 40 ns in Figure 3. This RMSD value indicates that the alkaloid class of hymenidin was tightly bound to the SARS-CoV-2 main protease and is in an acceptable range. According to [34], the cyclic depsipeptide of plitidepsin (from ascidian) with the SARS-CoV-2 main protease showed similar RMSD values with fluctuations around 0.3 nm at 300 K until 50 ns.

Root-mean-square fluctuation (RMSF) is similar to RMSD, and it is an important parameter to define the flexible areas of a protein–ligand system. It mainly involves individual amino acid residue flexibility. It is used to explore the conformation stability due to the individual amino acids of the SARS-CoV-2 main protease in the complex form with hymenidin. Fewer fluctuation coordinates represent more stability. The RMSF value of the SARS-CoV-2 main protease–hymenidin docked complex was calculated to be around 0.1 to 0.4 nm at 300 K temperature and 1 bar pressure in optimized conditions (Figure 3). The RMSD and RMSF for the SARS-CoV-2 main protease–hymenidin complex showed stable binding throughout 50 ns. The stable RMSD and RMSF showed that the hymenidin had a strong binding affinity to the SARS-CoV-2 main protease and may be reasonable to act as a good inhibitor against the SARS-CoV-2 main protease.

The radius of gyration (ROG) is a physical parameter used to calculate the distance between the center of mass of the protein (the SARS-CoV-2 main protease) taken with its rotational axis. The ROG analysis for the SARS-CoV-2 main protease with hymenidin was examined for 50 ns at 300 K temperature and 1 bar pressure in optimized conditions. The average value of ROG for hymenidin with the SARS-CoV-2 main protease was found to be around 2.1 to 2.2 nm (Figure 4). It represents the conformational stability of the

formed protein–ligand complex between the SARS-CoV-2 main protease and hymenidin. According to [42], commercial drugs (such as 5-fluorouracil, methotrexate, and paclitaxel) found similar ROG values around 2.0 to 2.2 nm. The H-bond interaction is important for docking studies. It can be classified into two types: conventional and non-conventional H-bonding. Non-conventional H-bonding plays a vital role in molecular docking studies [43] as the stability of the small molecule in the active binding region of the protein is calculated in terms of the average number of non-conventional H-bonds. In the present study, the docked complex formed a maximum of four H-bond interactions (Figure 4).
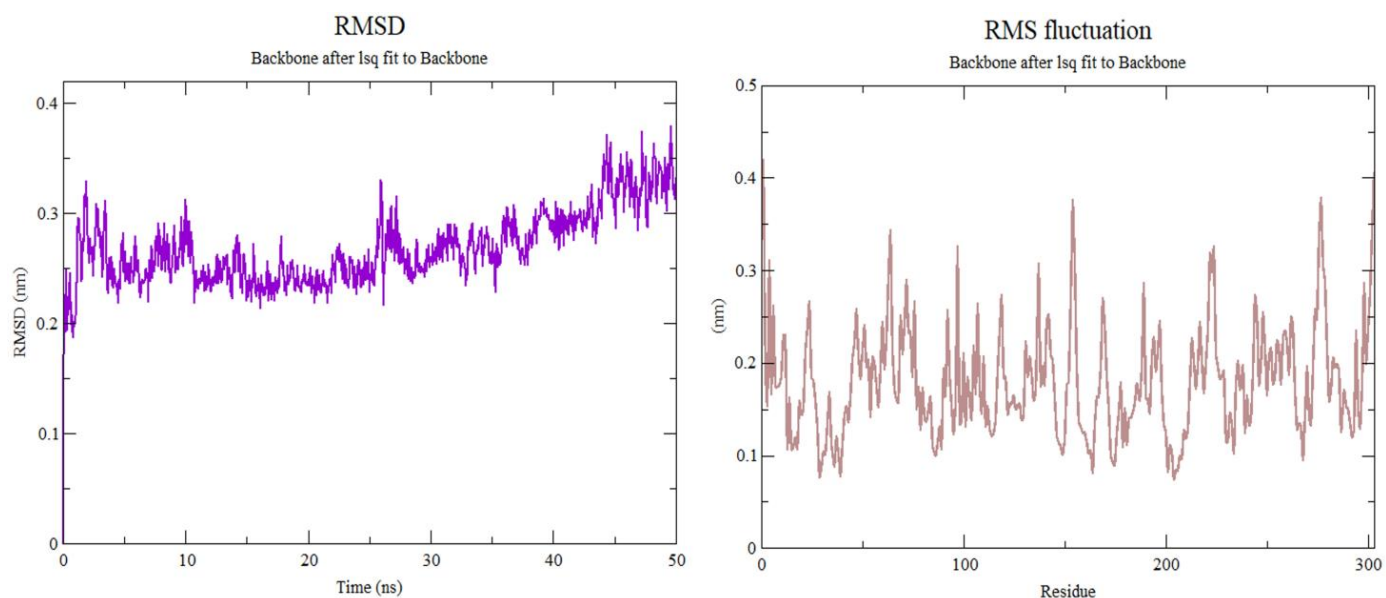

Figure 3. Root-mean-square deviation (RMSD) and RMS fluctuation values of hymenidin with the SARS-CoV-2 main protease during the entire 50 ns in MD.
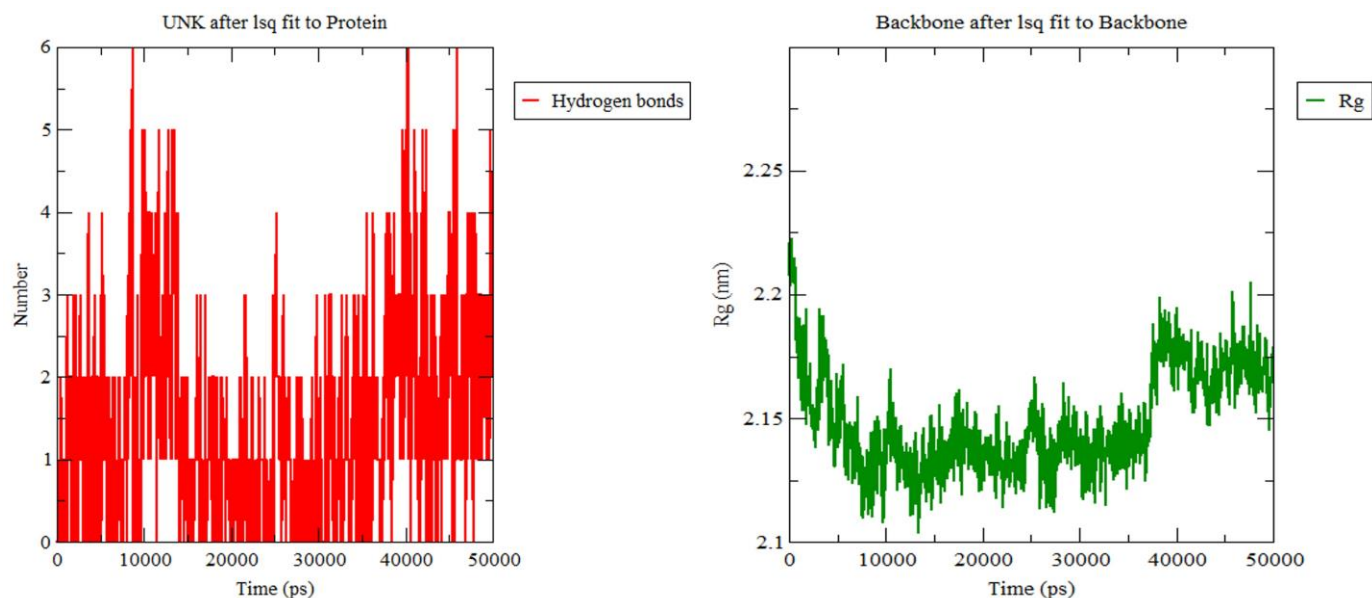

Figure 4. Trajectory of radius of gyration (ROG) and H-bond interaction for the SARS-CoV-2 main protease with hymenidin.

3.4. Pharmacokinetic Properties Analysis

In silico ADMET screening has been widely used in drug development and the drug discovery process. It is used to minimize failure rates and reduce the time of drug discovery.

Aqueous solubility, intestinal absorption, and membrane permeability are important criteria for the drug development process [44,45]. Aqueous solubility is an important criterion to study the ratio of drug uptake, transfer, and clearance. Gastrointestinal absorption (GIB) and drug distribution are major obstacles in oral drug delivery. A higher intestinal absorption value indicates that the drug has good bioavailability in the system. The five lead MDPs (chrysophaentin A, geodisterol sulfates, hymenidin, plinabulin (NPI-2358), tetrodotoxin) against COVID-19 targets were analyzed for ADMET properties using the pkCSM online server. The results of six active compounds with high activity potentials are represented in Table 4. More than 30% of GIB values implies good absorbance. Chrysophaentin A showed the highest percentage of GIB (100%), followed by hymenidin (71.26%) and plinabulin (65.66%) which showed good absorption scores. Geodisterol sulfates (49.98%) and tetrodotoxin (36.93%) displayed a moderate absorption percentage. A skin permeability (SKP) value greater than −2.5 cm/h is considered low skin permeability, and all five drug candidates showed acceptable SKP values. Similarly, all five drug candidates displayed low Caco2 permeability (<0.9 cm/s). P-glycoprotein (PGP) is an important drug transporter, and it helps to determine the uptake and efflux of a range of drugs. The inhibition of PGP can result in the increased bioavailability of the susceptible drug, and the induction of PGP reduces the bioavailability [46,47]. All five drug candidates were shown to be a substrate for PGP. Chrysophaentin A and geodisterol sulfates were both observed to be inhibitors for PGP.

The VDss, CNS, and BBB membrane permeability were used to study the drug distribution [48]. A value greater than log 0.45 represents a relatively higher distribution volume. All drug candidates exhibited less than log 0.45 value, and plinabulin exhibited the better VDss (0.325) compared to the other four compounds. The BBB membrane permeability (range: log BB values > 0.3) and CNS permeability (range of log PS values > −2 to < −3) are important parameters in the distribution mechanism. All five marine drug compounds were predicted to be neither capable of crossing the CNS nor BBB membranes. CYP450 plays a vital role in all drug metabolism, and it has two important subtypes: CYP2D6 and CYP3A4. All five compounds were not substrates for CYP2D6 [49], and similarly, all compounds were not substrates for CYP3A4 except chrysophaentin A. Chrysophaentin A, geodisterol sulfates, hymenidin, and tetrodotoxin CYP1A2 inhibitors were not predicted as substrates for the CYP2C19, CYP2C9, CYP2D6, CYP3A4 inhibitors. Plinabulin was predicted to be an inhibitor for CYP2C19 and CYP3A4. This suggested that chrysophaentin A and plinabulin may be metabolized in the liver.

Drug excretion is related to the MW and hydrophilicity of marine active compounds. There are two important parameters involved in drug excretion: (i) total clearance (TCs) and (ii) the renal OCT2 substrate. TCs is measured using a combination of hepatic and renal clearance [50]. Hymenidin (1.027) showed the highest TCs score followed by tetrodotoxin (0.663), plinabulin (0.457), and geodisterol sulfates (0.27), and chrysophaentin A (−0.211) showed the least TCs score. None of the compounds were predicted as a substrate for renal OCT2. Toxicity is an important role in the selection of the most suitable drug compounds. AMES toxicity is used to predict the carcinogenic effect of drug compounds [51]. None of the compounds expressed AMES toxicity except plinabulin. hERG inhibition (I and II) is an important parameter that is mainly involved in cardiotoxicity [52]. None of the marine drug compounds expressed inhibitory actions of the hERG-I channel. Chrysophaentin A and plinabulin were involved in inhibitory actions of the hERG-II channel. All compounds were predicted as they may not have skin sensitization and hepatotoxicity (except hymenidin). The maximum tolerated dose (for humans), LD50, and LOAEL values were predicted and are tabulated in Table 4. The lead five drug candidates have some drawbacks due to their functional and structural properties. Further molecular modification is required to obtain a potential antiviral drug against SARS-CoV-2.

Table 4. In silico ADMET/pharmacokinetic property analysis of the selected marine-derived clinical-level compounds using pkCSM web server.

Property	Name	Tetrodotoxin	Chrysophaentin A	Geodisterol Sulfates	Hymenidin	Plinabulin	Unit
Absorption	Water solubility	−2.244	−2.898	−3.231	−2.893	−2.894	log mol/L
	Caco2 permeability	0.557	−0.859	0.551	−0.336	−0.128	log Papp in 10⁻ cm/s
	Intestinal absorption (human)	36.93	100	49.98	71.261	65.663	% Absorbed
	Skin permeability	−2.735	−2.735	−2.735	−2.735	−2.735	log Kp
	P-glycoprotein substrate	Yes	Yes	Yes	Yes	Yes	Yes/No
	P-glycoprotein I inhibitor	No	Yes	No	No	No	Yes/No
	P-glycoprotein II inhibitor	No	Yes	Yes	No	No	Yes/No
Distribution	VDss (human)	−1.053	−1.24	−1.205	−0.367	0.325	log L/kg
	Fraction unbound (human)	0.8	0.143	0.08	0.458	0.101	Numeric (Fu)
	BBB permeability	−1.149	−2	−0.893	−1.288	−0.285	log BB
	CNS permeability	−5.174	−2.487	−2.763	−4.592	−2.619	log PS
Metabolism	CYP2D6 substrate	No	No	No	No	No	Yes/No
	CYP3A4 substrate	No	Yes	No	No	No	Yes/No
	CYP1A2 inhibitor	No	No	No	No	Yes	Yes/No
	CYP2C19 inhibitor	No	No	No	No	No	Yes/No
	CYP2C9 inhibitor	No	No	No	No	No	Yes/No
	CYP2D6 inhibitor	No	No	No	No	Yes	Yes/No
	CYP3A4 inhibitor	No	No	No	No	No	Yes/No
Excretion	Total clearance score	0.663	−0.211	0.27	1.027	0.457	log mL/min/kg
	Renal OCT2 substrate	No	No	No	No	No	Yes/No
Toxicity	AMES toxicity	No	No	No	No	Yes	Yes/No
	Max. tolerated dose (human)	0.44	0.432	−0.098	0.551	0.424	log mg/kg/day
	hERG I inhibitor	No	No	No	No	No	Yes/No
	hERG II inhibitor	No	Yes	No	No	Yes	Yes/No
	Oral rat acute toxicity (LD50)	2.061	2.512	2.686	2.507	2.669	mol/kg
	Oral at chronic toxicity	5.252	2.535	2.247	2.19	1.662	log mg/kg bw/day
	Hepatotoxicity	No	No	No	Yes	No	Yes/No
	Skin sensitization	No	No	No	No	No	Yes/No
	T.Pyriformis toxicity	0.285	0.285	0.285	0.285	0.285	log ug/L
	Minnow toxicity	7.311	−0.711	−0.305	2.477	4.67	log mM

Abbreviations: VDss: volume of distribution at steady state; BBB: brain–blood barrier; CNS: central nervous center; CYP: cytochrome P; OCT: organic cation transporter; hERG: human ether-a-go-go-related gene; LD50: lethal dose of 50%.

4. Conclusions

In summary, 16 marine-derived clinical-level compounds were investigated using in silico drug-likeness analysis, molecular docking, and ADMET properties. Among the 16 drug candidates, 5 compounds are proposed as potential hits against the SARS-CoV-2 main protease. In vitro, chrysophaentin inhibited MRSA, vancomycin-resistant *Enterococcus faecium*, and multidrug-resistant *Staphylococcus aureus*. The geodisterol sulfates also exhibited antibacterial activity against *Candida albicans*. Hymenidin inhibits HepG cytotoxicity activities. Tetrodotoxin was first reported as a molecular docking hit potential against SARS-CoV-2. The present study suggests that chrysophaentin A, hymenidin, and tetrodotoxin could be options to treat COVID-19-associated infections. Three compounds that were successful in binding to each of the targeted proteins were identified by the study and have shown stable behaviour, binding affinity, and molecular interactions. Our research discovered three compounds that were effective against each of the targeted proteins and showed stable behaviour, higher binding affinities, important residual molecular interactions, and good in silico pharmacokinetic properties. Overall, we suggest that these five compound hits might be promising pharmacological candidates for new COVID-19 treatments and suggest additional in vitro research on them.

References

1. Abd El-Aziz, T.M.; Stockand, J.D. Recent Progress and Challenges in Drug Development against COVID-19 Coronavirus (SARS-CoV-2)-an Update on the Status. *Infect. Genet. Evol.* **2020**, *83*, 104327. [CrossRef] [PubMed]
2. Idda, M.L.; Soru, D.; Floris, M. Overview of the First 6 Months of Clinical Trials for COVID-19 Pharmacotherapy: The Most Studied Drugs. *Front. Public Health* **2020**, *8*, 497. [CrossRef] [PubMed]
3. Prathiviraj, R.; Saranya, S.; Bharathi, M.; Chellapandi, P. A Hijack Mechanism of Indian SARS-CoV-2 Isolates for Relapsing Contemporary Antiviral Therapeutics. *Comput. Biol. Med.* **2021**, *132*, 104315. [CrossRef] [PubMed]
4. Prathiviraj, R.; Chellapandi, P.; Begum, A.; Kiran, G.S.; Selvin, J. Identification of Genotypic Variants and Its Proteomic Mutations of Brazilian SARS-CoV-2 Isolates. *Virus Res.* **2022**, *307*, 198618. [CrossRef] [PubMed]
5. Singh, M.; de Wit, E. Antiviral Agents for the Treatment of COVID-19: Progress and Challenges. *Cell Rep. Med.* **2022**, *3*, 100549. [CrossRef]
6. Li, H.; Xue, Q.; Xu, X. Involvement of the Nervous System in SARS-CoV-2 Infection. *Neurotox. Res.* **2020**, *38*, 1–7. [CrossRef]
7. Rahman, M.M.; Bibi, S.; Rahaman, M.S.; Rahman, F.; Islam, F.; Khan, M.S.; Hasan, M.M.; Parvez, A.; Hossain, M.A.; Maeesa, S.K.; et al. Natural therapeutics and nutraceuticals for lung diseases: Traditional significance, phytochemistry, and pharmacology. *Biomed. Pharmacother.* **2022**, *150*, 113041. [CrossRef]
8. Varga, Z.; Flammer, A.J.; Steiger, P.; Haberecker, M.; Andermatt, R.; Zinkernagel, A.S.; Mehra, M.R.; Schuepbach, R.A.; Ruschitzka, F.; Moch, H. Endothelial Cell Infection and Endotheliitis in COVID-19. *Lancet* **2020**, *395*, 1417–1418. [CrossRef]
9. Kim, D.; Lee, J.-Y.; Yang, J.-S.; Kim, J.W.; Kim, V.N.; Chang, H. The Architecture of SARS-CoV-2 Transcriptome. *Cell* **2020**, *181*, 914–921. [CrossRef]
10. Pal, M.; Berhanu, G.; Desalegn, C.; Kandi, V. Severe acute respiratory syndrome coronavirus-2 (SARS-CoV-2): An update. *Cureus* **2020**, *12*, e7423. [CrossRef]
11. Yoshimoto, F.K. The Proteins of Severe Acute Respiratory Syndrome Coronavirus-2 (SARS CoV-2 or n-COV19), the Cause of COVID-19. *Protein J.* **2020**, *39*, 198–216. [CrossRef] [PubMed]
12. Bibi, S.; Khan, M.S.; El-Kafrawy, S.A.; Alandijany, T.A.; El-Daly, M.M.; Yousafi, Q.; Fatima, D.; Faizo, A.A.; Bajrai, L.H.; Azhar, E.I. Virtual screening and molecular dynamics simulation analysis of Forsythoside A as a plant-derived inhibitor of SARS-CoV-2 3CLpro. *Saudi Pharm. J.* **2022**, *30*, 979–1002. [CrossRef] [PubMed]

13. Bianchi, M.; Benvenuto, D.; Giovanetti, M.; Angeletti, S.; Ciccozzi, M.; Pascarella, S. Sars-CoV-2 Envelope and Membrane Proteins: Differences from Closely Related Proteins Linked to Cross-Species Transmission. *BioMed Res. Int.* **2020**, *2020*, 4389089. [CrossRef] [PubMed]

14. Snijder, E.J.; Decroly, E.; Ziebuhr, J. Coronaviruses. *Adv. Virus Res.* **2016**, *96*, 59–126.

15. Jackson, C.B.; Farzan, M.; Chen, B.; Choe, H. Mechanisms of SARS-CoV-2 Entry into Cells. *Nat. Rev. Mol. Cell Biol.* **2022**, *23*, 3–20. [CrossRef]

16. Biswas, P.; Hasan, M.M.; Dey, D.; dos Santos Costa, A.C.; Polash, S.A.; Bibi, S.; Ferdous, N.; Kaium, M.; Rahman, M.D.; Jeet, F.K.; et al. Candidate antiviral drugs for COVID-19 and their environmental implications: A comprehensive analysis. *Environ. Sci. Pollut. Res.* **2021**, *28*, 59570–59593. [CrossRef]

17. Alanagreh, L.; Alzoughool, F.; Atoum, M. The Human Coronavirus Disease COVID-19: Its Origin, Characteristics, and Insights into Potential Drugs and Its Mechanisms. *Pathogens* **2020**, *9*, 331. [CrossRef]

18. Wu, C.; Liu, Y.; Yang, Y.; Zhang, P.; Zhong, W.; Wang, Y.; Wang, Q.; Xu, Y.; Li, M.; Li, X. Analysis of Therapeutic Targets for SARS-CoV-2 and Discovery of Potential Drugs by Computational Methods. *Acta Pharm. Sin. B* **2020**, *10*, 766–788. [CrossRef]

19. Salehi, B.; Sharifi-Rad, J.; Seca, A.M.; Pinto, D.C.; Michalak, I.; Trincone, A.; Mishra, A.P.; Nigam, M.; Zam, W.; Martins, N. Current Trends on Seaweeds: Looking at Chemical Composition, Phytopharmacology, and Cosmetic Applications. *Molecules* **2019**, *24*, 4182. [CrossRef]

20. Tanna, B.; Mishra, A. Nutraceutical Potential of Seaweed Polysaccharides: Structure, Bioactivity, Safety, and Toxicity. *Compr. Rev. Food Sci. Food Saf.* **2019**, *18*, 817–831. [CrossRef]

21. Dyshlovoy, S.A.; Honecker, F. Marine Compounds and Cancer: The First Two Decades of XXI Century. *Mar. Drugs* **2019**, *18*, 20. [CrossRef] [PubMed]

22. Kumar, L.D.; Prathiviraj, R.; Selvakumar, M.; Guna, R.; Abbirami, E.; Sivasudha, T. HRLC-ESI-MS Based Identification of Active Small Molecules from Cissus Quadrangularis and Likelihood of Their Action towards the Primary Targets of Osteoarthritis. *J. Mol. Struct.* **2020**, *1199*, 127048. [CrossRef]

23. Murugesan, S.; Srinivasan, V.; Lakshmanan, D.K.; Venkateswaran, M.R.; Jayabal, S.; Nadar, M.M.; Kathiravan, A.; Jhonsi, M.A.; Thilagar, S.; Periyasamy, S. Evaluation of the Anti-Rheumatic Properties of Thymol Using Carbon Dots as Nanocarriers on FCA Induced Arthritic Rats. *Food Funct.* **2021**, *12*, 5038–5050. [CrossRef] [PubMed]

24. Lipinski, C.A.; Lombardo, F.; Dominy, B.W.; Feeney, P.J. Experimental and Computational Approaches to Estimate Solubility and Permeability in Drug Discovery and Development Settings. *Adv. Drug Deliv. Rev.* **1997**, *23*, 3–25. [CrossRef]

25. Pires, D.E.; Blundell, T.L.; Ascher, D.B. PkCSM: Predicting Small-Molecule Pharmacokinetic and Toxicity Properties Using Graph-Based Signatures. *J. Med. Chem.* **2015**, *58*, 4066–4072. [CrossRef]

26. Selvakumar, M.; Palanichamy, P.; Arumugam, V.; Venkatesan, M.; Aathmanathan, S.; Krishnamoorthy, H.; Pugazhendhi, A. In Silico Potential of Nutraceutical Plant of Pithecellobium Dulce against GRP78 Target Protein for Breast Cancer. *Appl. Nanosci.* **2021**, 1–13. [CrossRef]

27. Abraham, M.J.; Murtola, T.; Schulz, R.; Páll, S.; Smith, J.C.; Hess, B.; Lindahl, E. GROMACS: High Performance Molecular Simulations through Multi-Level Parallelism from Laptops to Supercomputers. *SoftwareX* **2015**, *1*, 19–25. [CrossRef]

28. Tian, C.; Kasavajhala, K.; Belfon, K.A.; Raguette, L.; Huang, H.; Migues, A.N.; Bickel, J.; Wang, Y.; Pincay, J.; Wu, Q. Ff19SB: Amino-Acid-Specific Protein Backbone Parameters Trained against Quantum Mechanics Energy Surfaces in Solution. *J. Chem. Theor. Comput.* **2019**, *16*, 528–552. [CrossRef]

29. Salgarello, M.; Visconti, G.; Barone-Adesi, L. Interlocking Circumareolar Suture with Undyed Polyamide Thread: A Personal Experience. *Aesthetic Plast. Surg.* **2013**, *37*, 1061–1062. [CrossRef]

30. Hammad, S.; Bouaziz-Terrachet, S.; Meghnem, R.; Meziane, D. Pharmacophore Development, Drug-Likeness Analysis, Molecular Docking, and Molecular Dynamics Simulations for Identification of New CK2 Inhibitors. *J. Mol. Model.* **2020**, *26*, 160. [CrossRef]

31. Wang, J.; Wang, W.; Kollman, P.A.; Case, D.A. Automatic Atom Type and Bond Type Perception in Molecular Mechanical Calculations. *J. Mol. Graph. Model.* **2006**, *25*, 247–260. [CrossRef] [PubMed]

32. Yusof, I.; Segall, M.D. Considering the Impact Drug-like Properties Have on the Chance of Success. *Drug Discov. Today* **2013**, *18*, 659–666. [CrossRef] [PubMed]

33. Hu, Q.; Xiong, Y.; Zhu, G.-H.; Zhang, Y.-N.; Zhang, Y.-W.; Huang, P.; Ge, G.-B. The SARS-CoV-2 Main Protease (Mpro): Structure, Function, and Emerging Therapies for COVID-19. *MedComm* **2022**, *3*, e151. [CrossRef]

34. Vishvakarma, V.K.; Singh, M.B.; Jain, P.; Kumari, K.; Singh, P. Hunting the Main Protease of SARS-CoV-2 by Plitidepsin: Molecular Docking and Temperature-Dependent Molecular Dynamics Simulations. *Amino Acids* **2022**, *54*, 205–213. [CrossRef] [PubMed]

35. Bibi, S.; Hasan, M.M.; Wang, Y.B.; Papadakos, S.P.; Yu, H. Cordycepin as a Promising Inhibitor of SARS-CoV-2 RNA dependent RNA polymerase (RdRp). *Curr. Med. Chem.* **2022**, *29*, 152–162. [CrossRef] [PubMed]

36. Rauf, A.; Rashid, U.; Khalil, A.A.; Khan, S.A.; Anwar, S.; Alafnan, A.; Alamri, A.; Rengasamy, K.R. Docking-Based Virtual Screening and Identification of Potential COVID-19 Main Protease Inhibitors from Brown Algae. *S. Afr. J. Bot.* **2021**, *143*, 428–434. [CrossRef] [PubMed]

37. Ghosh, S.; Das, S.; Ahmad, I.; Patel, H. In Silico Validation of Anti-Viral Drugs Obtained from Marine Sources as a Potential Target against SARS-CoV-2 Mpro. *J. Indian Chem. Soc.* **2021**, *98*, 100272. [CrossRef]

38. Ramadhan, D.S.F.; Siharis, F.; Abdurrahman, S.; Isrul, M.; Fakih, T.M. In Silico Analysis of Marine Natural Product from Sponge (Clathria Sp.) for Their Activity as Inhibitor of SARS-CoV-2 Main Protease. *J. Biomol. Struct. Dyn.* **2021**, *40*, 11526–11532. [CrossRef]

39. Swain, S.S.; Singh, S.R.; Sahoo, A.; Panda, P.K.; Hussain, T.; Pati, S. Integrated Bioinformatics–Cheminformatics Approach toward Locating Pseudo-Potential Antiviral Marine Alkaloids against SARS-CoV-2-Mpro. *Proteins Struct. Funct. Bioinform.* **2022**, *90*, 1617–1633. [CrossRef]

40. Baildya, N.; Ghosh, N.N.; Chattopadhyay, A.P. Inhibitory Activity of Hydroxychloroquine on COVID-19 Main Protease: An Insight from MD-Simulation Studies. *J. Mol. Struct.* **2020**, *1219*, 128595. [CrossRef]

41. Krupanidhi, S.; Abraham Peele, K.; Venkateswarulu, T.C.; Ayyagari, V.S.; Nazneen Bobby, M.; John Babu, D.; Venkata Narayana, A.; Aishwarya, G. Screening of Phytochemical Compounds of Tinospora Cordifolia for Their Inhibitory Activity on SARS-CoV-2: An in Silico Study. *J. Biomol. Struct. Dyn.* **2021**, *39*, 5799–5803. [CrossRef] [PubMed]

42. Singh, M.B.; Vishvakarma, V.K.; Lal, A.A.; Chandra, R.; Jain, P.; Singh, P. A Comparative Study of 5-Fluorouracil, Doxorubicin, Methotrexate, Paclitaxel for Their Inhibition Ability for Mpro of NCoV: Molecular Docking and Molecular Dynamics Simulations. *J. Indian Chem. Soc.* **2022**, *99*, 100790. [CrossRef]

43. Chen, D.; Oezguen, N.; Urvil, P.; Ferguson, C.; Dann, S.M.; Savidge, T.C. Regulation of Protein-Ligand Binding Affinity by Hydrogen Bond Pairing. *Sci. Adv.* **2016**, *2*, e1501240. [CrossRef] [PubMed]

44. Aungst, B.J. Optimizing Oral Bioavailability in Drug Discovery: An Overview of Design and Testing Strategies and Formulation Options. *J. Pharm. Sci.* **2017**, *106*, 921–929. [CrossRef] [PubMed]

45. Bergström, C.A. In Silico Predictions of Drug Solubility and Permeability: Two Rate-Limiting Barriers to Oral Drug Absorption. *Basic Clin. Pharmacol. Toxicol.* **2005**, *96*, 156–161. [CrossRef]

46. Igel, S.; Drescher, S.; Mürdter, T.; Hofmann, U.; Heinkele, G.; Tegude, H.; Glaeser, H.; Brenner, S.S.; Somogyi, A.A.; Omari, T. Increased Absorption of Digoxin from the Human Jejunum Due to Inhibition of Intestinal Transporter-Mediated Efflux. *Clin. Pharmacokinet.* **2007**, *46*, 777–785. [CrossRef]

47. König, J.; Müller, F.; Fromm, M.F. Transporters and Drug-Drug Interactions: Important Determinants of Drug Disposition and Effects. *Pharmacol. Rev.* **2013**, *65*, 944–966. [CrossRef]

48. Han, Y.; Zhang, J.; Hu, C.Q.; Zhang, X.; Ma, B.; Zhang, P. In Silico ADME and Toxicity Prediction of Ceftazidime and Its Impurities. *Front. Pharmacol.* **2019**, *10*, 434. [CrossRef]

49. Bibi, Z. Role of Cytochrome P450 in Drug Interactions. *Nutr. Metab.* **2008**, *5*, 27. [CrossRef]

50. Shargel, L.; Wu-Pong, S.; Yu, A.B.C. Chapter 6. Drug Elimination and Clearance. In *Applied Biopharmaceutics & Pharmacokinetics*, 6th ed.; The McGraw-Hill Companies: New York, NY, USA, 2012; p. 106.

51. Kirkland, D.; Zeiger, E.; Madia, F.; Gooderham, N.; Kasper, P.; Lynch, A.; Morita, T.; Ouedraogo, G.; Morte, J.M.P.; Pfuhler, S. Can in Vitro Mammalian Cell Genotoxicity Test Results Be Used to Complement Positive Results in the Ames Test and Help Predict Carcinogenic or in Vivo Genotoxic Activity? I. Reports of Individual Databases Presented at an eurl ecvam Workshop. *Mutat. Res. Genet. Toxicol. Environ. Mutagen.* **2014**, *775*, 55–68. [CrossRef]

52. Creanza, T.M.; Delre, P.; Ancona, N.; Lentini, G.; Saviano, M.; Mangiatordi, G.F. Structure-Based Prediction of HERG-Related Cardiotoxicity: A Benchmark Study. *J. Chem. Inf. Model.* **2021**, *61*, 4758–4770. [CrossRef] [PubMed]